A Molecular Dynamics Simulation of Ultrathin Oxide Films on Silicon: Growth by Thermal O Atoms and Sputtering by 100 eV Ar$^+$ Ions

Alison Kubota and Demeter J. Economou

Abstract—**Molecular dynamics was applied to study the growth and sputtering of ultrathin oxide films on (100) Si surfaces. A multibody potential which stabilized the Si/SiO$_2$ interface was used for this purpose. Oxide growth by exposure to O atoms was found to follow Langmuir-type kinetics with unity initial sticking coefficient of O and saturation coverage of around four monolayers, in agreement with experimental data. Sputtering of an ultrathin oxide film on silicon by 100 eV Ar$^+$ ions was simulated to study ion-assisted surface cleaning. Ion irradiation was found to promote restructuring of the surface into oxide islands, as observed experimentally. Island formation was accompanied with an increase in surface roughness. The evolution of the surface state with ion dose was predicted quantitatively.**

Index Terms—**Molecular dynamics, oxide, simulation, surface cleaning, sputtering.**

I. INTRODUCTION

THE growth of thin oxide films on silicon is vital for fabricating metal-oxide-semiconductor (MOS) devices. Gate oxides are typically on the order of several tens of Å thick and are grown under high temperature conditions in an oxygen environment. They serve to passivate Si surface states and act as an insulating layer between silicon and the gate electrode. Many studies have been reported on the growth mechanism of oxide films and the structure of the Si/SiO$_2$ interface. There is evidence that growth occurs in a layer-by-layer fashion [1]–[4]. Langmuir and two-dimensional (2-D) island growth mechanisms have been identified, depending on the oxidation conditions [2], [5], [6].

In contrast, the native oxide which forms on Si as a result of prolonged exposure to ambient atmosphere is often a hindrance to many device fabrication steps. For example, epitaxial growth onto and plasma etching of Si both require smooth and clean substrates, free of oxides and other contaminants. In the Si etching case, surface micromasking by residual oxide can lead to the formation of surface roughness and unintentional topography. Typically, wet cleaning is employed to remove the native oxide and other surface contaminants. Dry processes such as energetic ion irradiation and high temperature annealing provide alternative means of

removing oxides. Hopper and coworkers [7], showed that flashing a Si sample above 1200 °C produces oxide-free and optically flat Si surfaces compared with ion-bombardment or ion-bombardment followed by annealing. However, such high substrate temperatures should be avoided to minimize dopant redistribution and defect generation which can degrade device performance. On the other hand, high energy ion irradiation can introduce significant surface roughness and damage. Lee and coworkers [8] have developed a silicon surface cleaning technique involving low energy noble gas ion irradiation. They showed that annealing at 700 °C *following* a 300 eV Ar$^+$ ion bombardment step resulted in clean, smooth, and well-ordered surfaces. However, they found that annealing at lower substrate temperatures (400–500 °C) while *simultaneously* irradiating by lower energy Ar$^+$ ions (100 eV) resulted in the same clean, smooth and well-ordered surface. The mechanism by which this synergism takes place is still an area of ongoing research.

II. COMPUTATIONAL METHODOLOGY

In this report, molecular dynamics (MD) was used to simulate the oxidation of Si by thermal O atoms, as well as cleaning (by sputtering) of ultrathin oxide films from Si surfaces by low energy ion irradiation. The effective interaction potential used was that of Jiang and Brown [9], [10], which combines the Stillinger and Weber [11] potential for Si with Kramer's [12] potential for silica. The empirical multibody form of the potential enables the simulation of silicon/oxygen structures which lie in the spectrum between pure Si and pure stoichiometric SiO2 by treating atomic charge and charge transfer as a function of the local instantaneous environment. Energetic Ar interactions were modeled with the purely repulsive Moliere potential.

The simulation cell was 11–16 Å high, composed of 8–12 Si monolayers (ML) oriented in the (001) direction. The lateral extent of the cell was 4 × 4 Si unit cells, with an exposed area of approximately 472 Å^2. The bottom two Si layers were fixed to bulk crystalline positions to prevent unphysical drift of the lattice and surface reconstruction of the bottom layers. To negate edge effects, periodic boundary conditions were applied in the lateral (x-y) directions. Each ion impact was integrated over approximately 3 ps, followed by 0.5 ps of equilibration. Any particles sputtered from the surface, as well as any remaining Ar, were removed prior to equilibration
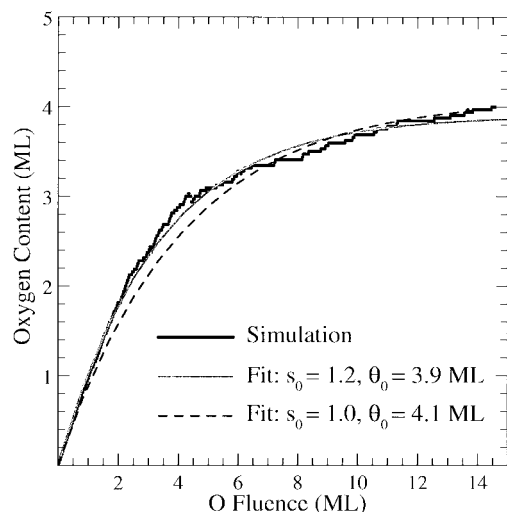
Fig. 1. O content of lattice in monolayers (ML), as a function of impinging O fluence (ML). Simulation results (darker solid line) are fit to a first-order Langmuir model (lighter solid line and dashed line).
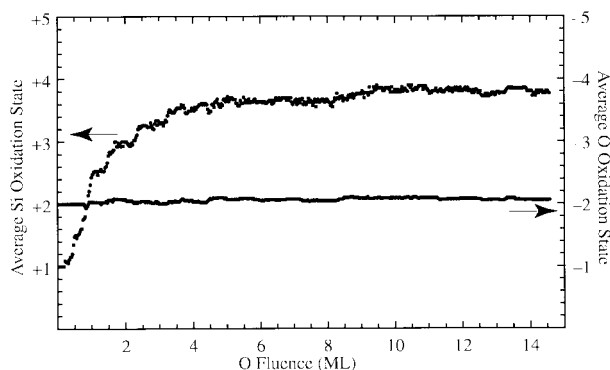

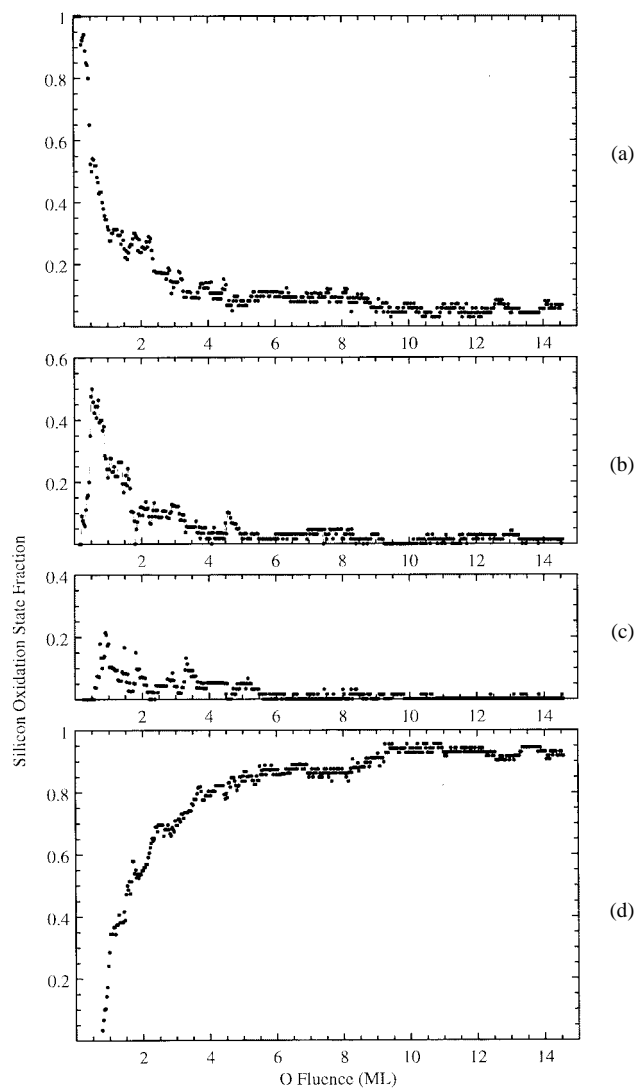Fig. 2. Average oxidation state of *charged* Si and O, as a function of O fluence in monolayers (ML).

Fig. 3. Fraction of charged Si atoms in different oxidation states ($+1$ to $+4$) as a function of O atom fluence in monolayers (ML). Shown are plots for (a) $+1$, (b) $+2$, (c) $+ 3$, and (d) $+4$ Si states.

and before further ion impacts. The heat-removal scheme of Berendsen [13] was applied to the lower 6 Å of the cell with a coupling constant of 10 fs at all times. However, during the equilibration phase, heat removal was applied to the entire lattice, coupled to a specified set-point temperature. A variable time-step velocity-Verlet integration scheme was applied with the value of the time-step determined adaptively according to the speed of the fastest atom. All simulations were performed on HP9000 735/125 RISC workstations. Further details of the computational methodology can be found elsewhere [14].

Ultrathin oxide films were formed by repeated bombardment of thermal energy O atoms onto an initially clean Si(100) (2X1) surface. O atoms were successively impacted from random positions above the lattice, while reflected O was removed at the end of each impact simulation. The surface was impacted until an oxide film consisting of roughly 4 ML of O was formed. However, an intermediate surface containing ~2.3 ML O was selected as the initial condition lattice for the sputtering simulations to match the initial O atom concentration of Lee *et al.* [8].

Oxide sputtering simulations involved the successive impact of 100 eV Ar$^+$ onto the surface from random positions above

the lattice. The following four cases were studied: Normally incident 100 eV Ar$^+$ with substrate temperatures 1) $T_s = 25$ °C, 2) $T_s = 300$ °C, 3) $T_s = 600$ °C, and 4) ions incident at 45° from normal with a substrate temperature of $T_s = 300$ °C. The evolution of the surface was monitored in terms of the cumulative quantity of O and Si removed from the lattice, the root-mean-square (RMS) surface roughness, the oxidation state distribution of O and Si atoms, and visual atomic configurations, all as a function of O (for growth) or Ar$^+$ ion (for sputtering) fluence. The cumulative O and Si were used as opposed to direct sputtering yield due to the dynamic nature of the surface.

The presence of oxide islands [15]–[17] on a silicon surface can lead to a significant increase in topographical roughness. Si adatoms on pristine Si surfaces are regarded as having sufficient mobility to cause surface relaxation to more flattened profiles [18]. Oxides, on the other hand, are highly networked SiO$_4$ tetrahedral units capable of stabilizing many shapes by distortion of the connectivity of the network. The RMS
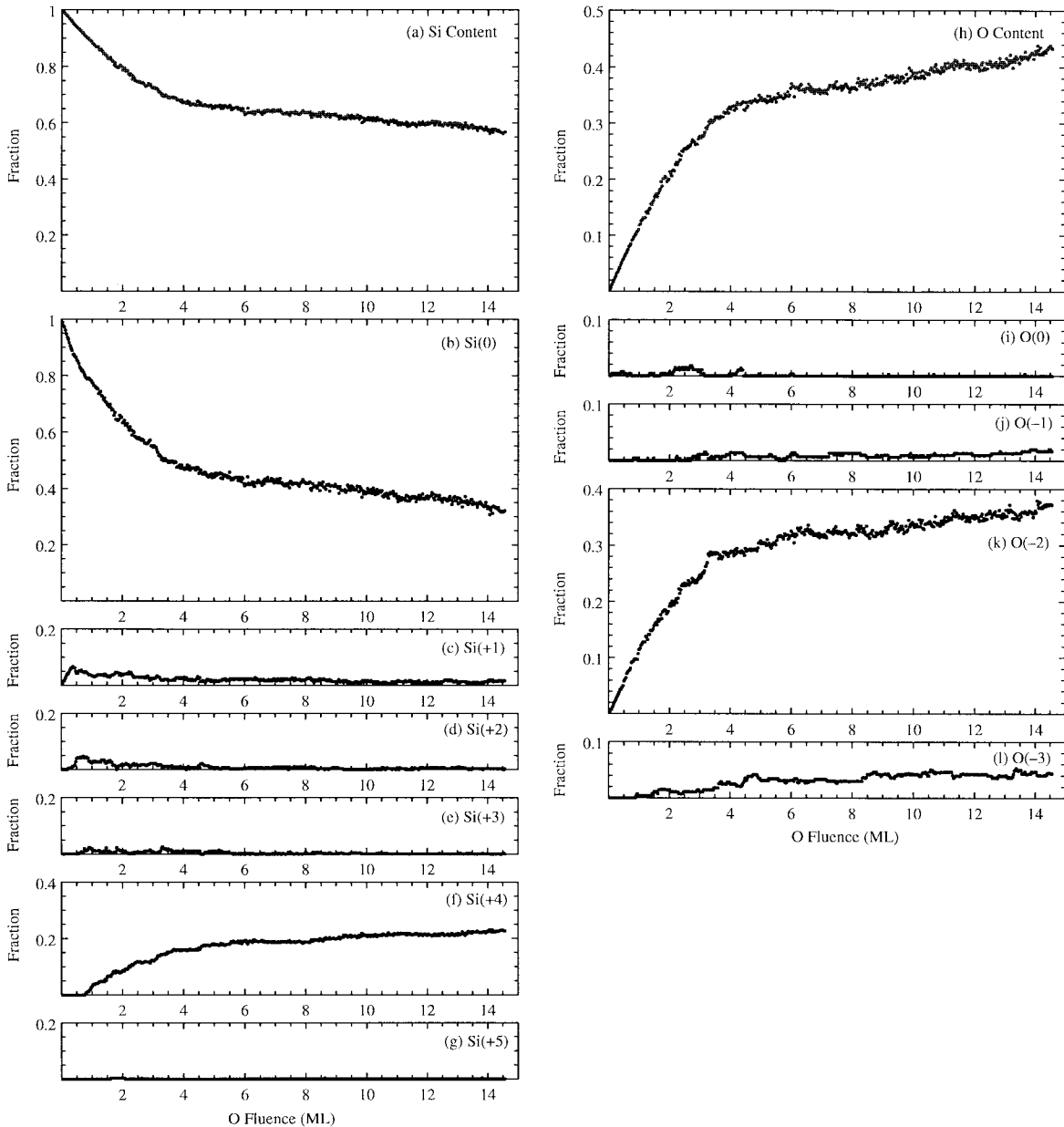
Fig. 4. Fraction of Si and O atoms and their oxidation states, sampled over the top 10 Å of the computational cell. All data is plotted as a function of atomic O fluence in monolayers (ML). Shown are plots for the (a) total Si content, (b) neutral, (c) +1, (d) +2, (e) +3, (f) +4, and (g) +5 Si oxidation states; (h) total oxygen content and (i) neutral, (j) −1, (k) −2, and (l) −3 O oxidation states.

roughness σ was calculated with

$$\sigma = \sqrt{\langle z^2 \rangle - \langle z \rangle^2} \qquad (1)$$

where z are cell heights as a function of lateral $(x\text{-}y)$ positions. The oxidation-state-distribution of atoms in and near the oxide layer gives information on the structure of the oxide and its interface. The oxidation state is tied directly to the formalism of the potentials. Oxidation state information is presented in several different forms. First, the average oxidation state of charged Si and O species is calculated to compare the stoichiometry and bonding coordination of the oxide layer to an ideal bulk oxide. Also the relative distribution of oxidation states is given. Finally the O and Si content and oxidation

state distributions sampled to a depth of 10 Å are given for comparison with XPS results of Lee and coworkers [8].

III. RESULTS AND DISCUSSION

A. Oxide Film Growth

Fig. 1 shows the oxygen content of the Si lattice in monolayers (ML) as a function of O fluence also in ML. One ML corresponds to 32 atoms for these simulations. The main feature of Fig. 1 is the rapid uptake of O with unity initial sticking probability which tapers off with increasing fluence. The uptake appears to follow approximately first-order Langmuir kinetics consistent with the study of Engstrom and
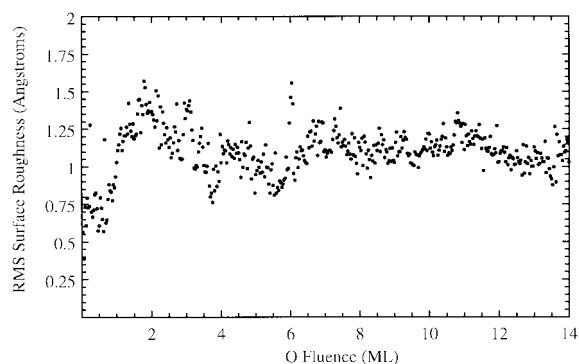
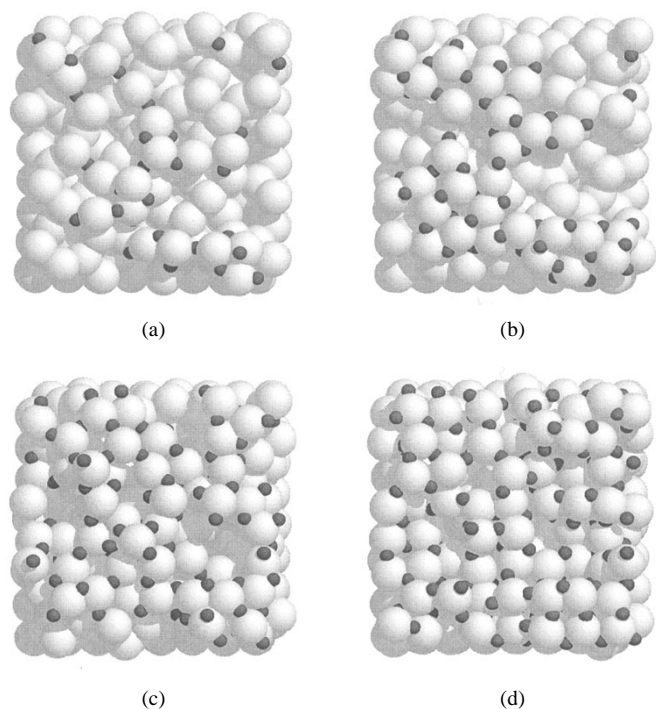Fig. 5. The RMS surface roughness as a function of O fluence in monolayers (ML).

Fig. 7. The initial condition lattice for the oxide sputtering study, consisting of approximately 2.3 ML of O on top of Si(100).

(a)   (b)

(c)   (d)

Fig. 6. Snapshots of a top view of the surface after (a) 1 ML, (b) 2 ML, (c) 4 ML, and (d) 12 ML of O fluence.

Fig. 8. The total and partial RDF of the oxidized silicon lattice: (a) O-O, (b) Si-O, (c) Si-Si, and (d) total RDF's are plotted versus interatomic distance.

coworkers [5] for atomic O interactions with initially clean Si. The corresponding first-order site-balance model is

$$\frac{d\theta}{dt} = s_o\left(I - \frac{\theta}{\theta_o}\right) \qquad (2)$$

where $\theta(t)$, the oxygen content in ML, is a function of the oxygen fluence t (in ML); s_0 and θ_0 are the initial sticking coefficient and oxygen saturation coverage in ML, respectively. Our data fit yields a saturation coverage of 3.9 ML, which compares well with 4.0 ML found by Engstrom et al. [5]. We obtain $\theta_0 = 4.1$ ML when s_0 is constrained to unity, but the Langmuir kinetics fit is degraded (Fig. 1). We take the initial sticking coefficient to be unity consistent with the findings of Engstrom and coworkers [5]. The ability for our computation to simulate the uptake of O and the formation of thin oxide layers on the short MD time-scale is due to the lack of energy barrier for atomic O chemisorption onto a clean Si
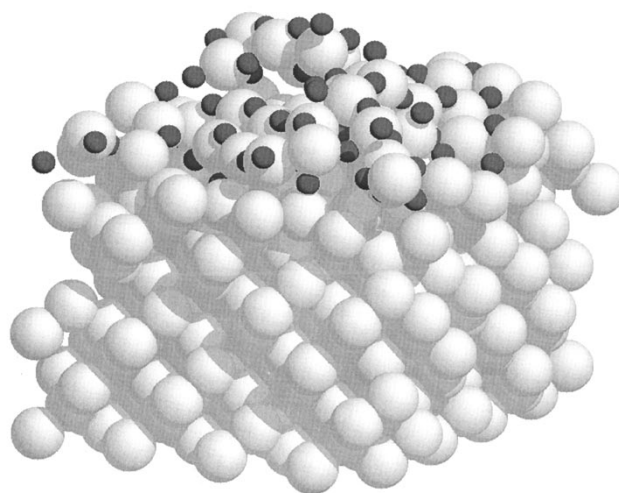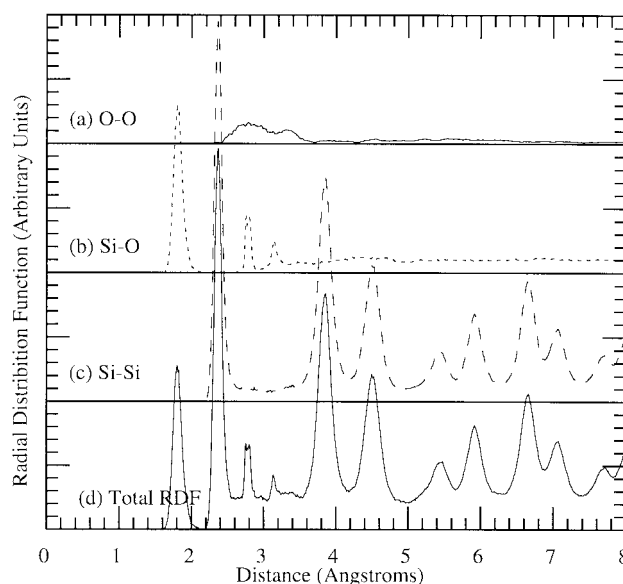
surface, compared with molecular O_2 chemisorption which has a sticking coefficient on the order of 0.01 [5], [17], [19], [20]. The more complicated pathway of O_2 chemisorption involves various physisorbed and chemisorbed states [20]–[23] with strong site and defect dependencies [24], [25] which accounts for the lower initial sticking coefficient.

At all stages of chemisorption, O appears to preferentially form O^{2-} by O insertion into Si-Si bridging sites. This too has been found to occur by Engstrom and coworkers [5], for atomic O adsorption. Fig. 2 shows the average oxidation state of *charged* Si and O (not including neutral states) in the simulation cell. The average oxidation state of O remains at approximately -2, independent of O fluence (and hence, O content). With increasing O fluence beyond 4 ML, the average Si oxidation state approaches $+4$ asymptotically. An average Si oxidation state less than $+4$ is attributed

TABLE I
SIMULATION CASES STUDIED. AN INCIDENT ANGLE
OF $0°$ DENOTES NORMALLY INCIDENT IONS

Case Study	Ion Energy (eV)	Incident Angle(°)	Substrate Temperature (°C)
1	100	0	25
2	100	0	300
3	100	0	600
4	100	45	300

Fig. 9. Cumulative O removed from the surface for the four different cases of oxide film sputtering as a function of Ar^+ ion fluence in monolayers (ML).

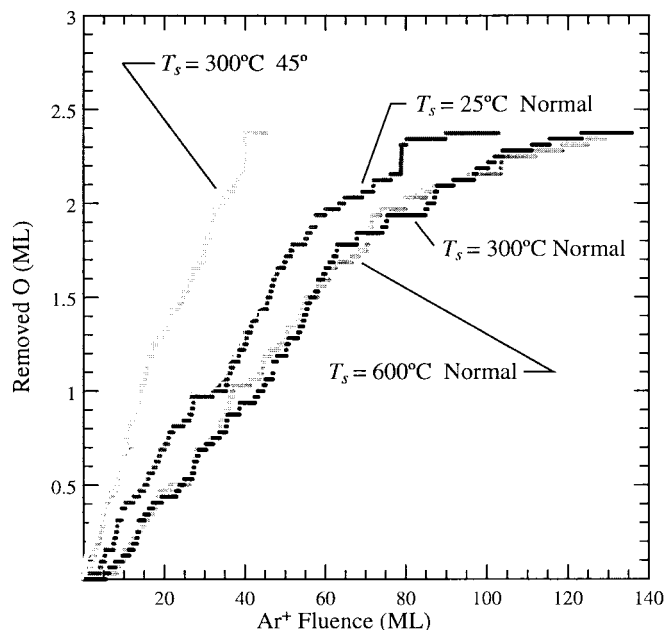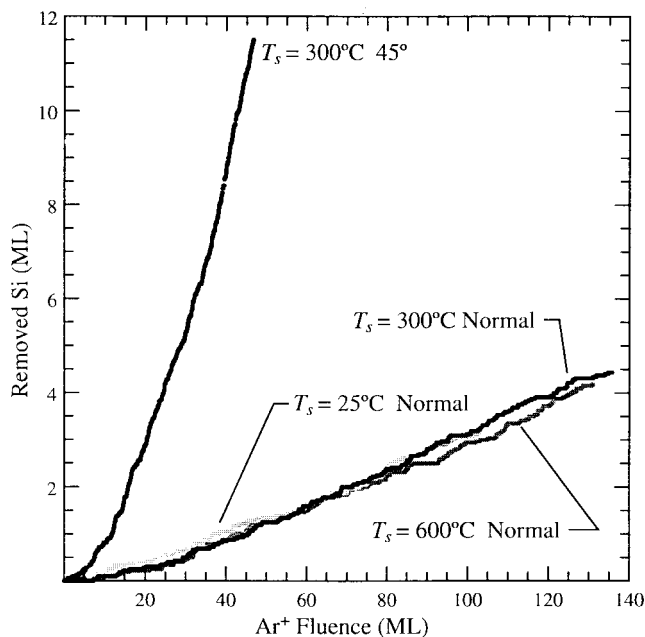
Fig. 10. Cumulative Si removed from the surface for the four different cases of oxide film sputtering as a function of Ar^+ ion fluence in monolayers (ML).

to Si sub-oxides concentrated at the Si/SiO$_2$ interface [24]. Fig. 3 shows the fraction of charged Si at different oxidation states as a function of O fluence. There are only $+1$ states initially with higher oxidation states observed as the O fluence increases. These results agree qualitatively with oxidation state distributions measured in ultrathin oxides (2–4 Å) by Ohishi and Hattori [3]. They observed a predominance of the $+1$ Si state initially. For an oxide approximately 2.1 Å thick, they observed $+1/+2/+3/+4$ oxidation state fractions of approximately 0.3/0.2/0.1/0.4, which agrees well with our simulation for O fluence of 1.5 ML, corresponding to an interpolated oxide of approximately 2–3 Å thick. At higher oxide thickness (higher O fluence), the Si^{+4} state dominates over intermediate Si oxidation states, with the $+1$ state fraction generally dominating over the $+2$ and $+3$ Si states. Above 4 ML O fluence, only the $+1$ and $+4$ states representing Si at the Si/SiO$_2$ interface and Si in the SiO$_2$ film, respectively, are present with a significant fraction. The decrease in the $+1$ Si fraction (and corresponding increase in the $+4$ Si fraction) is due to the continuous volume- and mass-growth of the oxide layer.

Fig. 4 shows the fractions of Si and O atoms and their oxidation states sampled over the top 10 Å of the computational cell. Fig. 4 (a)–(g) show silicon content and the total, neutral, $+1$, $+2$, $+3$, $+4$, and $+5$ Si oxidation states, respectively. Fig. 4

(h)–(l) show the oxygen content and the neutral, -1, -2, and -3 oxidation states, respectively. A monotonic decrease in total Si and increase in total O atoms is due to the uptake of O by the lattice. The continual decrease of total Si and increase of total O atom content again show that oxide growth continues even at O fluences > 6 ML. Furthermore, the significant fraction of charged Si and O attest to the oxidation of Si to form a stoichiometric oxide layer with the majority of Si and O with oxidation states of $+4$ and -2, respectively.

Fig. 5 reveals enhanced surface roughness due to O chemisorption. The RMS roughness increases drastically during the initial stages of oxidation (<2 ML O fluence) at which some surface restructuring occurs to form higher oxidation states of Si. Furthermore, Si atoms in the vicinity of chemisorbed O migrate toward the oxygen-rich regions, thus leaving exposed Si regions. This process appears to be the main contributor to the increased roughness observed in Fig. 5. With further oxidation however, a less rough oxide layer is formed which accounts for the reduced RMS roughness at higher O fluences as also shown in Fig. 6.

Fig. 6 shows top views of the lattice at various stages of oxide layer formation: after (a) 1 ML, (b) 2 ML, (c) 4 ML, and (d) 12 ML of O fluence. A significant increase in surface roughness from 1 ML fluence (1 ML O content) to 2 ML fluence (1.9 ML content) is observed, with the tendency to form some bulk-silica-coordinated oxide, apparent even after as little as 1 ML of O fluence. At the very initial stages of oxidation (fluence <1 ML), O is observed to chemisorb between Si atoms with significant distortion to the Si surface structure. Well-ordered backbond and dimer-bridging-site adsorbed oxygen as calculated by Uchiyama and Tsukada [27]–[29] were not observed probably because the MD time scales do not allow for sufficient relaxation of the lattice. After 4 ML O fluence, the exposed Si regions shrink
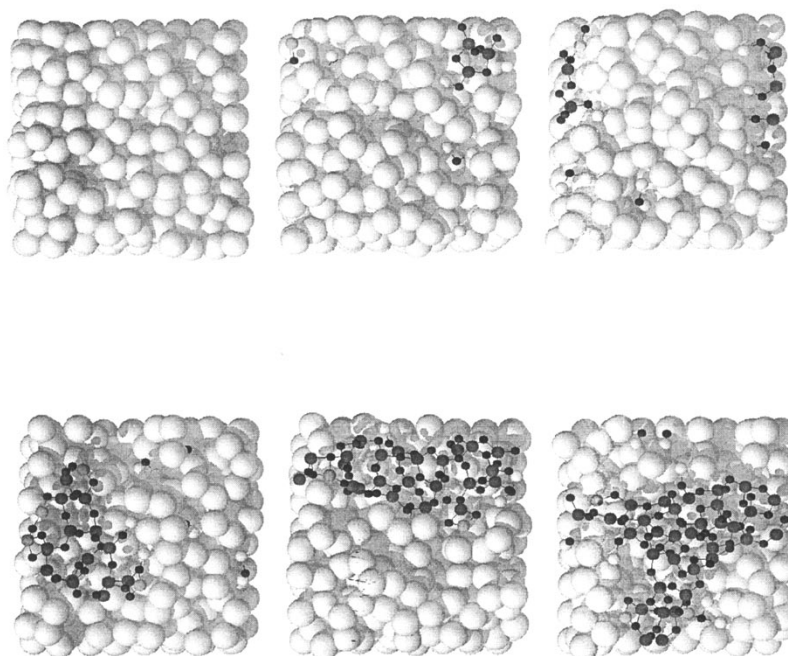
Fig. 11. Top view of the surface for the Case 1 study ($T_s = 25\,°C$, normally incident 100 eV Ar$^+$) after (top, left to right) 14, 28, 42, and (bottom, left to right) 56, 70, and 84 ML Ar$^+$ ion fluence in monolayers (ML).

[Fig. 6(c)] and are no longer present after 12 ML [Fig. 6(d)]. At this point, oxide growth appears to be quasi-self-limited, with the oxide film having a thickness of approximately 6.8 Å in reasonable agreement with a thickness of 5–6 Å calculated by Whidden and coworkers [30] and measured by Miura and coworkers [31] (6 Å thickness) and by Horie and coworkers [15] (7.1 Å thickness). However, it is apparent from Fig. 1 that the oxide layer continues to grow, albeit very slowly.

B. Oxide Film Sputtering

In this section, we discuss the results of oxide film sputtering by ion irradiation. The lattice used as the initial condition for oxide sputtering simulations is shown in Fig. 7. The top layer consists of approximately 2.3 ML of O which is rather uniformly distributed on the surface. This lattice approximates the initial O content that was used in the experiment of Lee *et al.* [8]. Fig. 8 shows the total and partial radial distribution functions (RDF) of the initial lattice. The Si-Si partial RDF agrees well with that of crystalline Si given by Leudtke and Landman [32]. The nearest and second nearest neighbor peaks are found at 2.4 and 3.9 Å, respectively. The highly peaked nature of the Si-Si partial RDF is due to the calculation performed over the entire lattice, much of which is composed of a crystalline Si phase. The Si-O contribution to the total RDF has a nearest neighbor peak at 1.8 Å, which is slightly higher than the expected value of 1.5–1.7 Å found for various polymorphs of silica [12], [33]–[45] and for chemisorbed O on Si [27], [28], [46]. Two additional peaks at 2.8 and 3.1 Å agree with the values of 2.7 and 3.1 Å from Garofalini [45].

The four different oxide sputtering cases studied are listed in Table I. The main parameter that measures the performance of surface cleaning is the remaining oxygen content of the lattice (or equivalently the cumulative quantity of O removed

from the lattice). Fig. 9 shows the cumulative O removed as a function of Ar$^+$ ion fluence. One monolayer constitutes 32 ions in this report. The vertical discontinuities indicate impacts resulting in multiple O or oxide cluster ejection. The O removal rate for normally incident 100 eV Ar$^+$ ions appears to be independent or weakly dependent on substrate temperature. Long time scale effects associated with annealing at different temperatures cannot be captured by MD. For normally incident ions and the three substrate temperatures studied (Case 1: $T_s = 25\,°C$, Case 2: $T_s = 300\,°C$ and Case 3: $T_s = 600\,°C$), the O sputtering yield (slope of the curves in Fig. 9) ranges from 0.02–0.04, for Ar$^+$ ion fluence below 50 ML. The O sputtering yield tapers off with increased ion fluence, due to depletion of O. Of course the sputtering yield data are only pointwise values corresponding to the simulation at hand. Many more simulations are needed to derive statistically significant sputtering yield values. In cases 1 and 4, a sharp discontinuity of the removed O is due to the fortuitous ejection of a small oxide cluster from the surface. In case 1, all O is observed to be removed after 80 ML Ar+ ion fluence. Cases 2 and 3 show all O to be removed after approximately 130 ML of Ar$^+$ ion fluence. When 45° incident Ar$^+$ ions are used in case 4, the initial O sputtering yield is enhanced to approximately 0.065 for ion fluence below 20 ML. In this case, O is completely removed from the surface after approximately 40 ML Ar$^+$ ion fluence, which compares well with approximately 45 ML from the study of Lee *et al.* [8] involving 100 eV Ar$^+$ at 45° incidence and substrate temperature of 400 °C. Their value of 45 ML is an upper limit to the required ion dose, since the effect of ion fluence on oxide cleaning performance was not followed. We show below that the oxidized surface undergoes significant changes in structure due to ion irradiation.
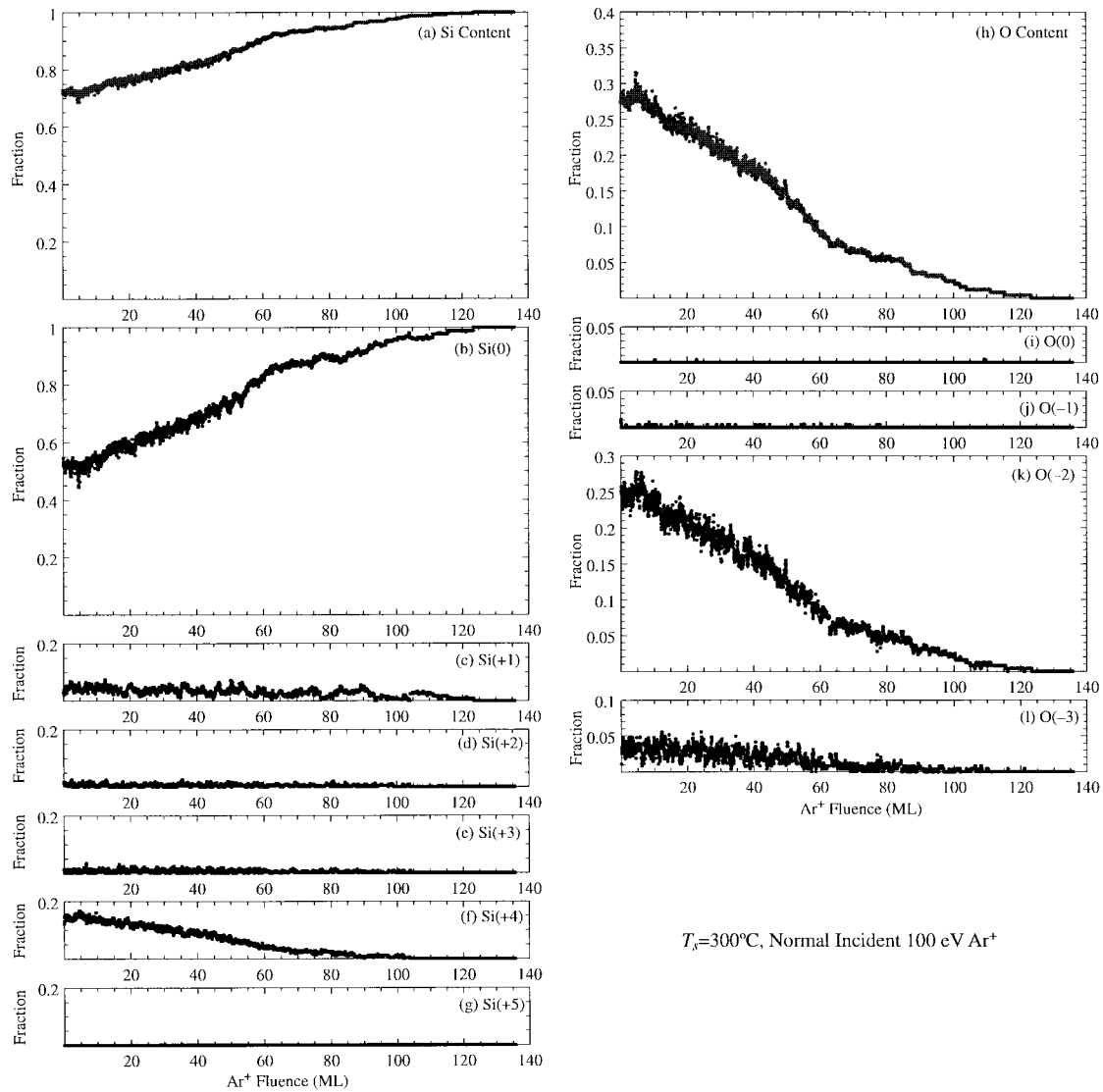
Fig. 12. Atomic concentrations (atom fraction) of Si and O and their oxidation states for the case 2 study ($T_s = 300$ °C, normally incident 100 eV Ar^+) study as a function of Ar^+ ion fluence in monolayers (ML). (a) Si content, (b) Si(0), (c) Si(+1), (d) Si(+2), (e) Si(+3), (f) Si(+4), (g) Si(+5), (h) O content, (i) O(0), (j) O(−1), (k) O(−2), and (l) O(−3).

Fig. 10 shows the cumulative Si removed as a function of Ar^+ fluence for the four cases discussed here. Again, there appears to be no temperature effect of the Si removal rate. The sputtering yields for cases 1–3 are approximately 0.02 for ion fluences below 30 ML, where the surface is partially covered by oxide film. With increasing ion fluence, the Si sputtering yield shows a slow increase to a value of approximately 0.03 which compares well with computationally [47], [48] and experimentally [49] found bare Si sputtering yields. In case 4 (ions impacting at 45°), the Si sputtering yield is increased, as expected.

Fig. 11 shows the top-view snapshots of the lattice for case 1 after 14 ML, 28 ML, 42 ML, 56 ML, 70 ML, and 84 ML Ar^+ ion fluence. The largest light-gray spheres are Si with zero oxidation state. Smaller light gray spheres represent Si with +1 to +5 oxidation states. The dark spheres represent O atoms. Oxygen atoms with higher absolute magnitudes of

oxidation state (up to $|-3|$) are shown darker than lower oxidation state O (down to $|-1|$). It is clear from Fig. 11 that the surface tends to form oxide clusters with repeated ion irradiation. After 14 ML Ar^+ ion fluence, the oxide is mainly stoichiometric, that is, mainly consisting of Si^{4+} and O^{2-}. Suboxides, or oxides consisting of Si^{1+}, Si^{2+}, and Si^{3+} are localized between the oxide and the Si surface as well as near individual O interstitials. Most O is in the −2 oxidation state. Due to the periodic boundary conditions applied to the limited-size cell, the oxide islands are often seen in the form of a band (top middle lattice). The islands are not pinned to specific sites on the surface, but shift in position with continuing ion irradiation. More than one islands have also been observed in the simulations, despite the limited cell size. Especially for oblique ion incidence (45° impact), small strands are occasionally formed on the surface which, upon further ion impacts, are peeled off to form metastable dangling
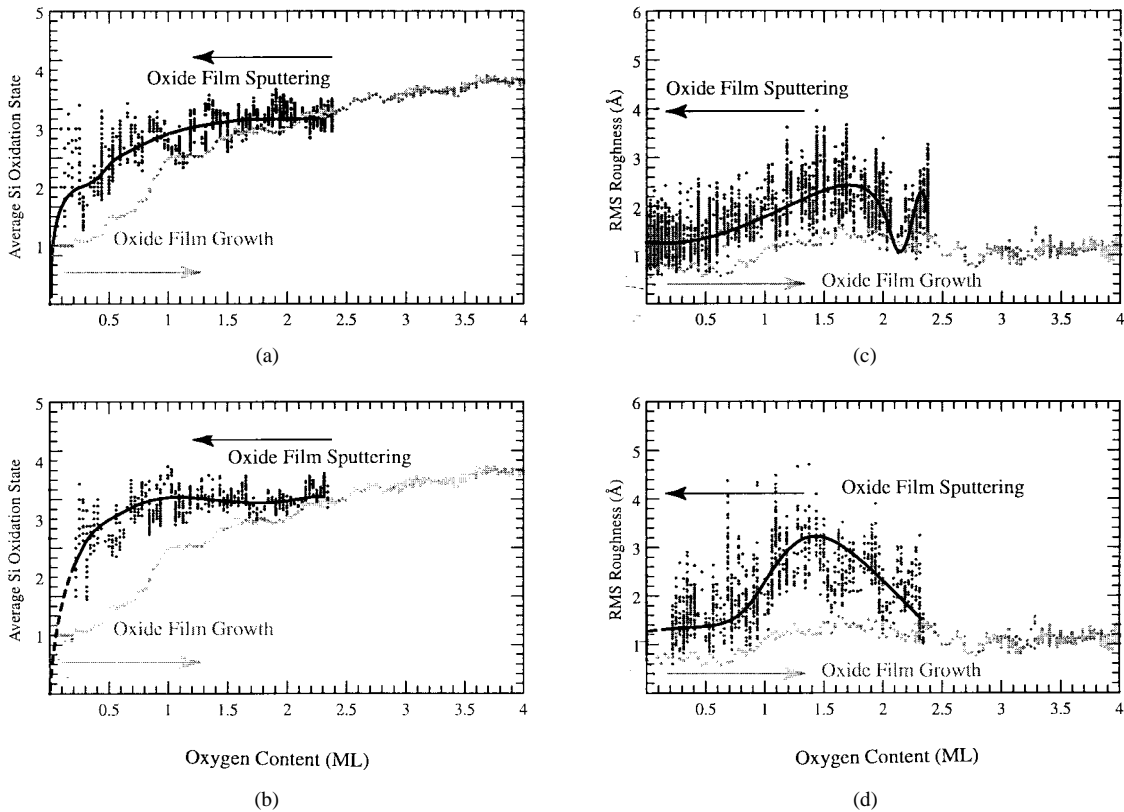
Fig. 13. Average Si oxidation state (left panels), and RMS surface roughness (right panels), for Cases 2 ($T_s = 300°C$, normally incident 100 eV Ar^+) and 4 ($T_s = 300°C$, 45° incident 100 eV Ar^+), as a function of O content of the lattice. In each case, data for both oxide growth (lighter dots) and oxide sputtering (darker dots) are shown.

structures [50]. Subsequent ion impacts can cause the oxide strands to cleanly eject from the surface, thus accounting for the discontinuities observed in Fig. 9.

Fig. 12 shows the atomic concentrations (atom fraction) of Si and O and their oxidation states for the case 2 impact sequence. The increasing total Si atomic concentration in Fig. 12(a) is due to a corresponding decrease in O with increasing ion fluence. The main contribution to the Si atom fraction is from neutral Si due to the large sampling depth of 10 Å, compared with an oxide film thickness of a few Å. However, of the charged species, Si^{4+} is initially the largest contributor. With increasing ion irradiation, the O^{2-} and Si^{4+} concentrations show a steady decrease. However, the Si^{1+} concentration appears to remain stable over the first 60 ML of Ar^+.

In Fig. 13 we show the average Si oxidation state and surface roughness for Cases 2 and 4, as a function of the O content. Data for both oxide film growth (lighter dots) and sputtering (darker dots) are shown. The solid curve is plotted to guide the eye, with the dashed section to fill in the missing data (the missing data is due to the ejection of oxide clusters). All plots of Fig. 13 show a hysteresis which is looped by the growth and sputtering phases. Although the growth phase data extend up to 4 ML of oxygen content, the sputtering data is only available up to 2.3 ML, the O content of the surface chosen as the initial condition lattice for this phase. The hysteresis loop is more pronounced for 45° incident ions.

We speculate that the lower average Si oxidation state for normally incident ions is due to the ability of O to be recoiled deeper below the surface and form suboxides. With an ion incident angle of 45°, the ability to maintain the suboxide structure is diminished, increasing the probability of oxide cluster ejection. Maxima observed in the RMS roughness plots during oxide sputtering are due to the reordering of the initially smooth oxide layer (see also Fig. 11) into coalesced islands. With decreasing O content, the reduced RMS roughness is mainly determined by the increasingly exposed Si.

IV. SUMMARY

MD was applied to study oxidation of Si by thermal energy O atoms using the multibody potential of Jiang and Brown [9], [10]. This potential was successfully applied to simulate ultrathin oxide films on silicon, in which both SiO_2 and Si phases as well as the SiO_2/Si interface region are stabilized. Oxide growth was found to follow approximately Langmuir-type kinetics with unity initial sticking coefficient of O and saturation coverage of around four monolayers, in agreement with experimental data.

Furthermore, cleaning of a 2.3 Å-thick oxide film on silicon by sputtering using 100 eV Ar^+ ion bombardment was simulated. Substrate temperature was found not to affect surface cleaning. However, diffusive phenomena which depend on temperature occur over much longer time scales than can be captured by MD. Ion irradiation was found to promote the

restructuring of the surface into distinct oxide islands with a corresponding increase in surface roughness. The evolution of the surface with ion impact was calculated quantitatively in terms of the oxidation state of surface and interface atoms, atomic concentrations, and RMS roughness.

REFERENCES

[1] M. Nishida, Y. Matsui, M. Okuyama, and Y. Hamakawa, "*In-situ* characterization of Si surface oxidation by high-sensitivity infrared reflection spectroscopic method," *Jpn. J. Appl. Phys. Part 1*, vol. 32, pp. 286–289, 1993.

[2] Y. Enta, Y. Takegawa, M. Suemitsu, and N. Miyamoto, "Growth kinetics of thermal oxidation process on Si(100) by real time ultraviolet photoelectron spectroscopy," *Appl. Surf. Sci.*, vol. 100/101, pp. 449–453, 1996.

[3] K. Ohishi and T. Hattori, "Periodic changes in SiO$_2$/Si(111) interface structures with progress on thermal oxidation," *Jpn. J. Appl. Phys. Part 1*, vol. 33, pp. L675–L678, 1994.

[4] F. M. Ross, J. M. Gibson, and R. D. Twesten, "Dynamic observations of interface motion during the oxidation of silicon," *Surf. Sc.*, vol. 310, pp. 234–266, 1994.

[5] J. R. Engstrom, D. J. Bonser, and T. Engel, "The reaction of atomic oxygen with Si(100) and Si(111). II, adsorption, passive oxidation and the effect of coincident ion bombardment," *Surf. Sci.*, vol. 268, pp. 238–264, 1992.

[6] Y. Takegawa, Y. Enta, M. Suemitsu, N. Miyamoto, and H. Kato, "Growth mode and characteristics of the O2-oxidized Si(100) surface oxide layer observed by real time photoemission measurement," *Jpn. J. Appl. Phys. Part 1*, vol. 37, pp. 261–265, 1998.

[7] M. A. Hopper, R. A. Clarke, and L. Young, "Removal of oxide films from silicon surfaces in a high vacuum system: An *in situ* ellipsometric study," *Surf. Sci.*, vol. 56, pp. 472–481, 1976.

[8] S. M. Lee, C. J. Fell, D. Marton, and J. W. Rabalais, "Synergistic effects in annealing and low energy ion bombardment of Si(100) surfaces," *J. App. Phys.*, vol. 83, pp. 5217–5223, 1998.

[9] Z. Jiang and R. A. Brown, "Modeling oxygen defects in silicon crystals using an empirical interatomic potential," *Chem. Eng. Sci.*, vol. 49, no. 17, pp. 2991–3000, 1994.

[10] ———, "Atomistic calculation of oxygen diffusivity in crystalline silicon," *Physical Rev. Lett.*, vol. 74, pp. 2046–2049, 1995.

[11] F. H. Stillinger and T. A. Weber, "Computer simulation of local order in condensed phases of silicon," *Physical Rev. B*, vol. 31, pp. 5262–5271, 1985.

[12] G. J. Kramer, N. P. Farragher, B. W. H. van Beest, and R. A. van Santen, "Interatomic force fields for silicas, aluminophosphates, and zeolites: Derivation based on ab initio calculations," *Physical Rev. B*, vol. 43, pp. 5068–5080, 1991.

[13] H. J. C. Berendsen, J. P. M. Postma, W. F. van Gunsteren, A. DiNola, and J. R. Haak, "Molecular dynamics with coupling to an external bath," *J. Chem. Phys.*, vol. 81, pp. 3684–3690, 1984.

[14] N. A. Kubota, "Molecular dynamics simulations of plasma-surface interactions for microelectronics processing applications," Ph.D. dissertation, Univ. Houston, Dept. Chem. Eng., Aug. 1998.

[15] T. Horie, Y. Takakuwa, and N. Miyamoto, "Two-dimensional growth and decomposition of initial thermal SiO2 layer on Si(100)," *Jpn. J. Appl. Phys.*, vol. 33, pp. 4684–4690, 1994.

[16] A. Feltz, U. Memmert, and R. J. Behm, "High temperature scanning tunneling microscopy studies on the interaction of O2 with Si(111)-(7 $\times$ 7) surfaces," *Surf. Sci.*, vol. 314, pp. 34–56, 1994.

[17] J. V. Seiple and J. P. Pelz, "Evolution of atomic-scale roughening on Si(001)-(2 $\times$ 1) surfaces resulting from high temperature oxidation," *J. Vacuum Sci. Technol. A*, vol. 13, pp. 772–776, 1995.

[18] H. Feil, J. Dieleman, and B. J. Garrison, "Chemical sputtering of Si related to roughness formation of a Cl-passivated Si surface," *J. Appl. Physi.*, vol. 74, pp. 1303–1309, 1993.

[19] H. D. Hagstrum, "Oxygen adsorption on silicon and germanium," *J. Appl. Phys.*, vol. 32, pp. 1020–1023, 1961.

[20] M. P. D'Evelyn, M. M. Nelson, and E. Thomas, "Kinetics of the adsorption of O2 and of the desorption of SiO on Si(100): A molecular beam, XPS and ISS study," *Surf. Sci.*, vol. 186, pp. 75–114, 1987.

[21] T. Miyake, S. Soeki, H. Kato, T. Nakamura, A. Namiki, H. Kamba, and T. Suzaki, "Molecular-beam study of sticking of oxygen on Si(100)," *Physical Rev. B*, vol. 42, pp. 11801–11807, 1990.

[22] T. Miyake, S. Soeki, H. Kato, T. Nakamura, A. Namiki, H. Kamba, and T. Suzaki, "Molecular beam study on scattering and sticking of molecular oxygen at Si(100)," *Surf. Sci.*, vol. 242, pp. 386–393, 1991.

[23] P. Avouris, I.-W. Lyo, and F. Bozso, "Atom-resolved surface chemistry: The early steps of Si(111)-7 $\times$ 7 oxidation," *J. Vacuum Sci. Technol. B*, vol. 9, pp. 424–430, 1991.

[24] M. Udagawa, Y. Umetani, H. Tanaka, M. Itoh, T. Uchiyama, Y. Watanabe, T. Yokotsuka, and I. Sumita, "The initial stages of the oxidation of Si(100)2 $\times$ 1 studied by STM," *Ultramicroscopy*, vols. 42–44, pp. 946–951, 1992.

[25] P. Avouris and D. Cahill, "STM studies of Si(100)-2 $\times$ 1 oxidation: Defect chemistry and Si ejection," *Ultramicroscopy*, vol. 42–44, pp. 838–844, 1992.

[26] Z. H. Lu, M. J. Graham, S. P. Tay, D. T. Jiang, and K. H. Tan, "Effects of growth temperature on the SiO$_2$/Si(100) interface structure," *J. Vacuum Sci. Technol. B*, vol. 13, pp. 1626–1629, 1995.

[27] T. Uchiyama and M. Tsukada, "Atomic and electronic structures of oxygen-adsorbed Si(001) surfaces," *Surf. Sci.*, vol. 357–358, pp. 509–513, 1996.

[28] ———, "Scanning-tunneling-microscopy images of oxygen adsorption on the Si(001) surface," *Physical Rev. B*, vol. 55, pp. 9356–9359, 1997.

[29] ———, "Atomic and electronic structures of oxygen-adsorbed Si(001) surfaces," *Physical Rev. B*, vol. 53, pp. 7917–7922, 1996.

[30] T. K. Whidden, P. Thanikasalam, M. J. Rack, and D. K. Ferry, "Initial oxidation of silicon (100): A unified chemical model for thin and thick oxide growth rates and interfacial structure," *J. Vacuum Sci. Technol. B*, vol. 13, pp. 1618–1625, 1995.

[31] T.-A. Miura, M. Niwano, D. Shoji, and N. Miyamoto, "Initial stages of oxidation of hydrogen-terminated Si surface stored in air," *Appl. Surface Sci.*, vol. 100/101, pp. 454–459, 1996.

[32] W. D. Leudtke and U. Landman, "Preparation, structure, dynamics, and energetics of amorphous silicon: A molecular-dynamics study," *Physical Rev. B*, vol. 40, pp. 1164–1174, 1989.

[33] R. W. G. Wyckoff, *Crystal Structure*, 2nd ed. New York: Interscience, 1965.

[34] L. Incoccia, A. Balerna, S. Cramm, C. Kunz, F. Senf, and I. Storjohann, "The adsorption site of oxygen on Si(100) determined by SEXAFS," *Surf. Sci.*, vol. 189/190, pp. 453–458, 1987.

[35] L. V. Woodcock, C. A. Angell, and P. Cheeseman, "Molecular dynamics studies of the vitreous state: Simple ionic systems and silica," *J. Chem. Phy.*, vol. 65, pp. 1565–1576, 1976.

[36] R. G. Della Valle and H. C. Andersen, "Molecular dynamics simulation of silica liquid and glass," *J. Chem. Phys.*, vol. 97, pp. 2682–2689, 1992.

[37] S. Tsuneyuki, M. Tsukuda, and H. Aoki, "First-principles interatomic potentials of silica appied to molecular dynamics," *Physical Rev. Lett.*, vol. 61, pp. 869–872, 1988.

[38] J. R. Rustad, D. A. Yuen, and F. J. Spera, "Molecular dynamics of liquid SiO$_2$ under high pressure," *Physical Rev. A*, vol. 42, pp. 2081–2089, 1990.

[39] ———, "Molecular dynamics of amorphous silica at very high pressures (135 GPa): Thermodynamics and extraction of structures through analysis of voronoi polyhedra," *Physical Rev. B*, vol. 44, pp. 2108–2121, 1991.

[40] D. Anderson, J. Kieffer, and S. Klarsfield, "Molecular dynamic simulations of the infrared dielectric response of silica structures," *J. Chem. Phys.*, vol. 98, pp. 8978–8986, 1993.

[41] S. K. Mitra, "Molecular dynamics simulation of silicon dioxide glass," *Philos. Mag. B*, vol. 45, no. 5, pp. 529–548, 1982.

[42] S. M. Levine and S. H. Garofalini, "A structural analysis of the vitreous silica surface via a molecular dynamics computer simulation," *J. Chem. Phys.*, vol. 86, pp. 2997–3002, 1987.

[43] B. P. Feuston and S. H. Garofalini, "Topological and bonding defects in vitreous silica surfaces," *J. Chem. Phys.*, vol. 91, pp. 564–570, 1989.

[44] ———, "Empirical three-body potential for vitreous silica," *J. Chem. Phys.*, vol. 89, pp. 5818–5824, 1988.

[45] S. H. Garofalini, "A molecular dynamics simulation of the vitreous silica surface," *J. Chem. Phys.*, vol. 78, pp. 2069–2072, 1983.

[46] A. Pasquarello, M. S. Hybertsen, and R. Car, "First-principles study of Si 2p core-level shifts at water and hydrogen covered Si(001) 2 × 1 surfaces," *J. Vacuum Sci, Technol, B*, vol. 14, pp. 2809–2816, 1996.

[47] N. A. Kubota and D. J. Economou, "Molecular dynamics simulations of low-energy (25–200 eV) argon ion interactions with silicon surfaces: Sputter yields and product formation pathways," *J, Appl, Phys.*, vol. 83, pp. 4055–4063, 1998.

[48] R. Smith, D. E. Harrison Jr., and B. J. Garrison, "keV particle bombardment of semiconductors: A molecular-dynamics simulation," *Phys. Rev. B*, vol. 40, pp. 93–101, 1989.

[49] D. J. Oostra, A. Haring, R. P. van Ingen, and A. E. de Vries, "Mechanisms of sputtering of Si in a Cl2 environment by ions with energies down to 75 eV," *J. Appl. Phys.*, vol. 64, pp. 315–322, 1988.

[50] N. A. Kubota and D. J. Economou, "Molecular dynamics simulations of ion-induced rearrangement of ultrathin oxide films on silicon," *IEEE Trans. Plasma Sci.*, vol. 27, pp. 106–107, Feb. 1999.

Alison Kubota received the B.S. degree in 1994 from the University of California at Berkeley and the Ph.D. degree in 1998 from the University of Houston, specializing in computational simulations of low energy ion-surface interactions.

Currently, she is a Postdoctoral Researcher at Lawrence Livermore National Laboratory, Livermore, CA.

Demeter J. Economou, for photograph and biography, see this issue, p. 1224.